nature geoscience

ARTICLES

https://doi.org/10.1038/s41561-018-0157-x

Atmospheric mountain wave generation on Venus and its influence on the solid planet's rotation rate

T. Navarro[1]*, G. Schubert[1] and S. Lebonnois[2]

The Akatsuki spacecraft observed a 10,000-km-long meridional structure at the top of the cloud deck of Venus that appeared stationary with respect to the surface and was interpreted as a gravity wave. Additionally, over four Venus solar days of observations, other such waves were observed to appear in the afternoon over equatorial highland regions. This indicates a direct influence of the solid planet on the whole Venusian atmosphere despite dissimilar rotation rates of 243 and 4 days, respectively. How such gravity waves might be generated on Venus is not understood. Here, we use general circulation model simulations of the Venusian atmosphere to show that the observations are consistent with stationary gravity waves over topographic highs—or mountain waves—that are generated in the afternoon in equatorial regions by the diurnal cycle of near-surface atmospheric stability. We find that these mountain waves substantially contribute to the total atmospheric torque that acts on the planet's surface. We estimate that mountain waves, along with the thermal tide and baroclinic waves, can produce a change in the rotation rate of the solid body of about 2 minutes per solar day. This interplay between the solid planet and atmosphere may explain some of the difference in rotation rates (equivalent to a change in the length of day of about 7 minutes) measured by spacecraft over the past 40 years.

A major surprise in the recent exploration of Venus has been the detection by the Akatsuki spacecraft of a planetary-scale temperature perturbation at the top of the cloud layer (65 km altitude)[1]. This structure is stationary with the surface, despite the discrepancy between the rotation of the surface and the superrotation of the cloud deck, with rotation periods of 243 and 4 days, respectively[2]. The perturbation is stationary, located above the equatorial elevated terrain of Aphrodite and shaped like a bow. These elements suggest that it corresponds to a mountain wave[1], a particular type of atmospheric gravity wave induced by topography. However, this perturbation is 10,000 km long in the meridional direction, a puzzling, huge extent never seen before in any planetary atmosphere. Furthermore, the altitude of observation at the cloud top contradicts at first glance our knowledge of the vertical structure of the Venusian atmosphere. Indeed, there is a neutral layer at the bottom of the cloud deck[2] that would not allow the vertical propagation of a gravity wave. Even more mysterious is the appearance of this wave on the dayside alone, generally in the afternoon[3].

To investigate the physical origin of this observation, we conducted a study with a numerical model of the atmosphere of Venus. We ran simulations of the Institut Pierre-Simon Laplace (IPSL) Venus general circulation model (GCM)[4,5], a full-physics model taking into account all known physical phenomena taking place in the atmosphere of Venus (see Methods). The initial state is obtained after convergence of the angular momentum over hundreds of days of simulation[5].

A planetary-scale structure as seen by Akatsuki has never been produced by a GCM, the IPSL Venus GCM included. The only exception is a simulation produced by a rather crude model of the atmosphere[1] that was produced after the discovery of the structure and obtained a gravity wave exhibiting a striking resemblance to the observations. However, this simulation included neither a parameterization of the physics (radiative transfer, convection), nor topography, and an arbitrary perturbation was imposed at 10 km of altitude of unphysical origin as the source of the gravity wave. Nevertheless, it opened the possibility that a more advanced, comprehensive numerical model might be able to obtain similar results with added realism, with the advantage to point out the physical mechanisms involved.

Planetary-scale gravity waves reproduced by modelling

The IPSL Venus GCM is utilized with a latitude–longitude grid with a resolution of 96 by 96 points; a 96 by 96 points on a latitude–longitude grid; hence, the horizontal resolution at the equator is approximately 200 km in the meridional direction and 400 km in the zonal direction. The topography of Venus shows variations at a much shorter horizontal scale, so that the topography used in the GCM is substantially smoothed. To resolve mountains and slopes at a finer scale that could play a role in the formation of mountain waves, one solution could be to increase the horizontal resolution, but the simulations would be too computationally intensive, prohibiting any long-term global simulation. Instead, we implemented a subgrid-scale parameterization of the topography, as is usually done for Earth[6–8] and Mars[9,10] studies. An adaptation of existing subgrid schemes for the case of Venus is necessary though. The usual rationale of a subgrid scheme is that gravity waves exist below the model resolution, and their effect on the flow has to be parameterized. Here, we simulate a gravity wave far greater than the model resolution, but for which the source is smaller than the resolution. To differentiate waves that reach the model resolution from the ones that stay at a subgrid scale, we consider the intensity of the mountain stress (see Methods).

In Fig. 1, the results with the IPSL Venus GCM and the newly included parameterization of subgrid topography show large-scale gravity waves, over four high topographic equatorial regions (Aphrodite Terra, Phoebe Regio, Beta Regio and Atla Regio),

[1]Department of Earth, Planetary, and Space Sciences, University of California, Los Angeles, CA, USA. [2]Laboratoire de Météorologie Dynamique (LMD/IPSL), Sorbonne Universités, UPMC Univ. Paris 6, ENS, PSL Research University, École Polytechnique Université Paris Saclay, CNRS, Paris, France.
*e-mail: tnavarro@epss.ucla.edu

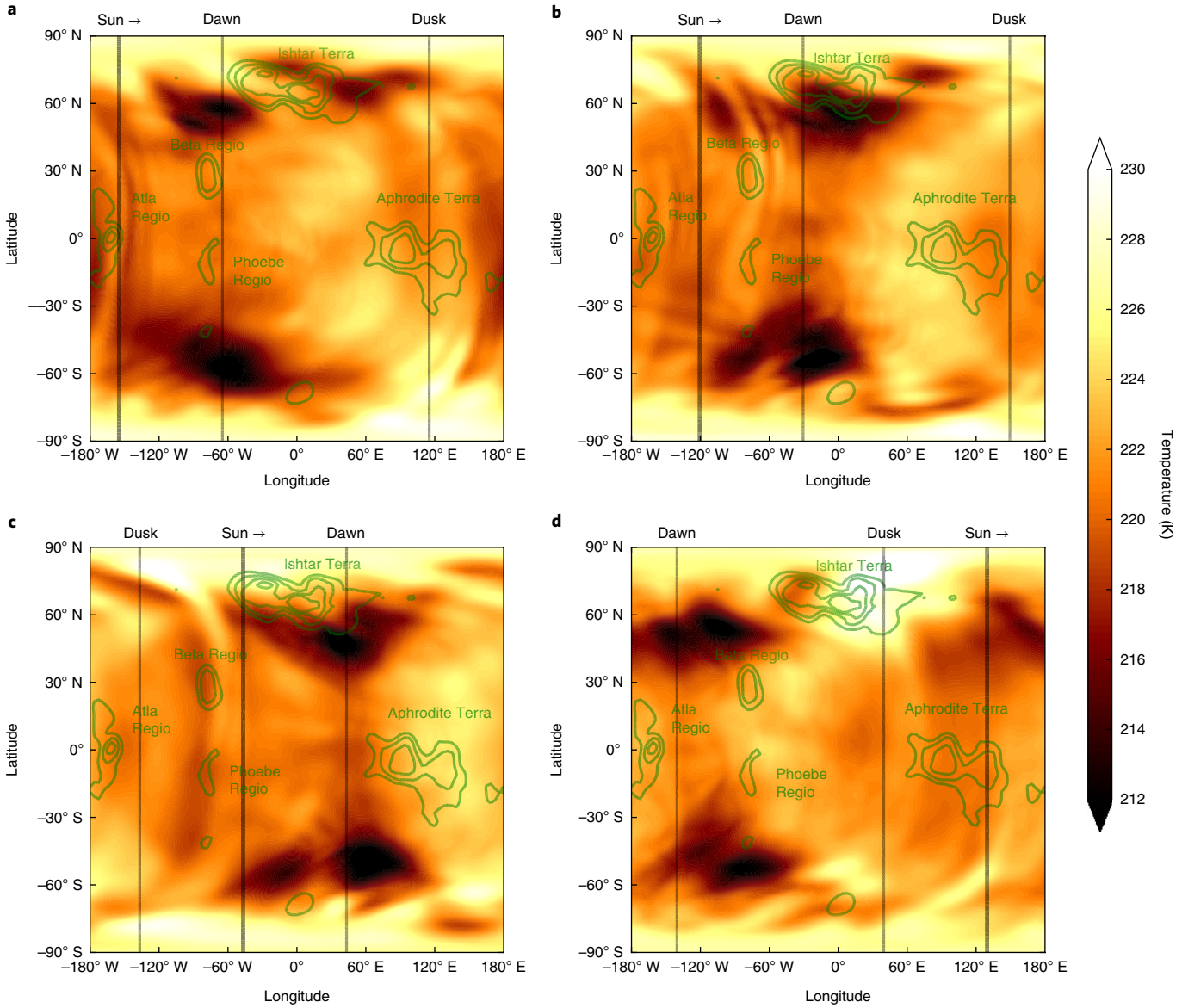

Fig. 1 | Planetary-scale gravity waves simulated with a GCM. a–d, Simulated temperature at the cloud top (70 km altitude) 8 (**a**), 19 (**b**), 43 (**c**) and 100 (**d**) Earth days after the beginning of the simulation. Mountain waves are seen as bow-shaped temperature disturbances. Topography is indicated in contours at altitudes 1, 2, 3 and 4 km. Supplementary Fig. 8 shows similarly the vertical and zonal winds.

a remarkable agreement with the observations over four Venus solar days from 2015 to 2017[3] (see also the Supplementary Movie).

At the cloud top (here, at 70 km in the GCM), the perturbation in temperature ranges from 1 to 3 K, a value similar to the observed 3 K perturbation in brightness temperature seen by Akatsuki. The cloud top is known to vary with latitude[11], and this structure is very similar at altitudes between 60 and 70 km.

Mechanism of the mountain wave generation

A notable aspect of the simulation is the dependence of mountain waves on local time, as seen in observations[3]. They appear in the simulation around noon, persist throughout the afternoon and quickly vanish with dusk. The exception is Beta Regio, where the wave appears earlier in the morning, in line with observations[3]. Overall, the behaviour with local time is very repeatable over the two Venus solar days of simulation.

All other things being equal, the mountain stress is maximum for $N = UH^{-1}$, where N is the near-surface Brunt–Väisälä frequency, H is the mountain height and U is the near-surface horizontal wind (see detailed explanations in the Supplementary Information). Stability conditions cause the mountain stress to be maximum during the afternoon (Supplementary Fig. 1).

In Fig. 2, this behaviour is illustrated with the example of Aphrodite Terra. As the Sun rises, the surface temperature increases slightly by 2 K, decreasing the near-surface stability N. As a result, the whole flow from the bottom of the mountain is able to pass the ridge and the blocked flow vanishes. The thickness of the gravity wave flow is limited by H. As the stability increases again in the afternoon due to mixing in the boundary layer, the mountain stress increases to a value of 5 Pa, with a maximum value in the afternoon. When the sun sets, the conditions are very stable, and most of the flow is blocked.

A second effect plays a role in the local time dependence of the total mountain stress. In the afternoon, the horizontal near-surface wind is greater, due to convective motions in the boundary layer, with a maximum value typically of 3 m s^{-1}, generating the planetary-scale gravity waves. In increased stable conditions at

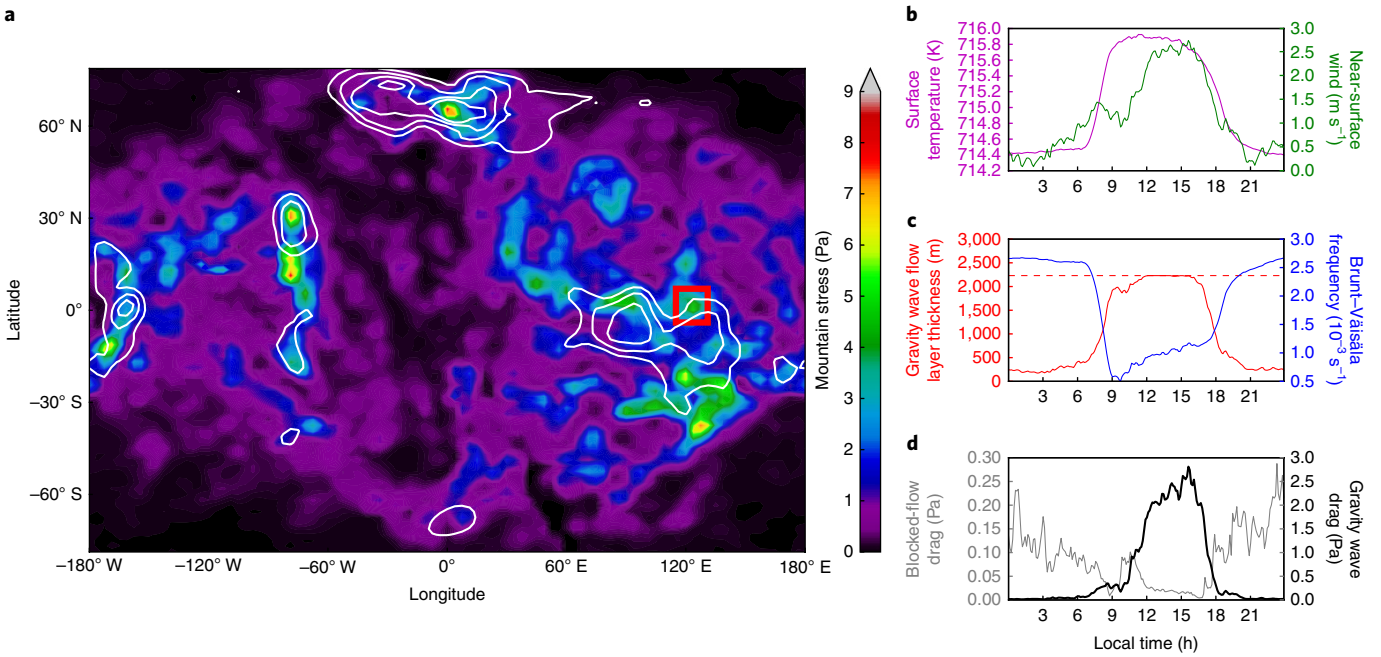

Fig. 2 | Surface conditions. a, Map of the maximum value of the mountain stress for two Venus solar days of simulation. **b**–**d**, Illustrative example over Aphrodite Terra (red box in **a**) as a function of local time. Topography is the same as in Fig. 1.

night or in the morning, the wind is less than 1 m s^{-1}. Hence, the maximal value of the blocked flow stress is substantially smaller than the maximal value of the gravity wave stress. This result differs from Earth, where generally a significant part of the total mountain stress is due to the blocked flow[12].

Over Beta Regio, the wave appears earlier in the day than for the other locations, in both observations and the simulations. The earliest occurrence of the wave from Akatsuki observations is 11:00, and 7:00 in the simulations. This early occurrence can be explained by the higher latitude of Beta Regio at 30° N, where two different effects play a complementary role to produce a strong surface stress earlier in the morning. First, the near-surface winds are stronger due to the jet present at the mid-latitudes, but absent at the equator (Supplementary Fig. 3). Second, the diurnal cycle of surface temperature and zonal wind is weaker at the latitude of Beta Regio than at the equator (Supplementary Fig. 3). The weaker diurnal cycle over Beta Regio limits the drop of stability in the morning, while sustained zonal winds persist in the morning (Supplementary Fig. 2). All in all, the morning conditions are such that a mountain wave is seen above Beta Regio, but not the equatorial mountains.

Atmospheric torque and length of day

The mountain stress at the subgrid scale creates a torque by the atmosphere on the solid body, never accounted for in previous studies of Venus. As seen in Fig. 3, the total torque exerted by the atmosphere can be split into a mountain torque and a friction torque[4]. Additional terms, of unphysical origin and model-dependent, are the residual tendency from the dynamical core, and, not shown here, the sponge layer torque and the dissipation torque.

It is worth noting that the highest regions of Venus, Ishtar Terra, located northward of 60° N, do not create planetary-scale gravity waves because they are disrupted by the wind shear of the polar vortex. However, Ishtar Terra has the highest mountain stress of the whole planet with a maximum of 8.5 Pa (Fig. 2). The torque exerted by the atmosphere on Ishtar Terra is nevertheless quite small, since this mountain range is located closer to the rotation axis than the equatorial ones.

In a simulation without the subgrid parameterization, the total torque fluctuates around zero, with values of typically $\pm 5.10^{19}$ kg m^2 s^{-2}. When the subgrid parameterization is implemented, there is a substantial additional term of mountain torque by unresolved mountains, with two fundamental characteristics. First, the subgrid mountain torque is positive on average, since the flow interacting with mountains tends to be in the same direction as the superrotation. The positive net torque indicates a transient response from one equilibrium (without subgrid parameterization) to the other (with parameterization). However, this transient response leads to an unrealistic state of the atmosphere, with retrograde winds, as detailed below and in the Supplementary Information. Second, the subgrid mountain torque peaks whenever high topographic regions (Aphrodite Terra, Beta Regio, Phoebe Regio and Atla Regio) are in the afternoon quadrant, associated with the presence of a planetary-scale gravity wave.

The budget of torques is given in Table 1, with $\mathrm{d}M/\mathrm{d}t + \mathrm{GW} + T + F + \epsilon + S + D = 0$, where M is the total atmospheric angular momentum, GW is the subgrid mountain torque, T is the resolved mountain torque, F is the friction torque, ϵ is the residual from conservation errors in the dynamical core, and S and D are the residual torques due to the sponge layer at the top of the model and the dissipation[13]. The terms S and D are negligible in this equation[13].

Without the subgrid parameterization, the total atmospheric angular momentum is quite stable, although it varies within a solar day. Sixteen years apart, the Magellan and Venus Express missions measured a length of day (LOD) difference of 7 minutes[14]. This long-term trend can be partially explained by the intradiurnal change of LOD due to atmospheric motions. The effect of the atmosphere on the LOD changes is comparable to the effect of the tidal torque exerted by the Sun on the solid body, in contrast to the conclusion that the LOD variations are due entirely to the solid-body torque[15]. The reason for this revised atmosphere-induced LOD change is the resolved mountain torque variability, which is higher than in previous simulations due to recent improvements of the IPSL GCM[5], in particular horizontal resolution. The fluctuation of surface pressure, and thus of the resolved mountain torque, is mostly due to two

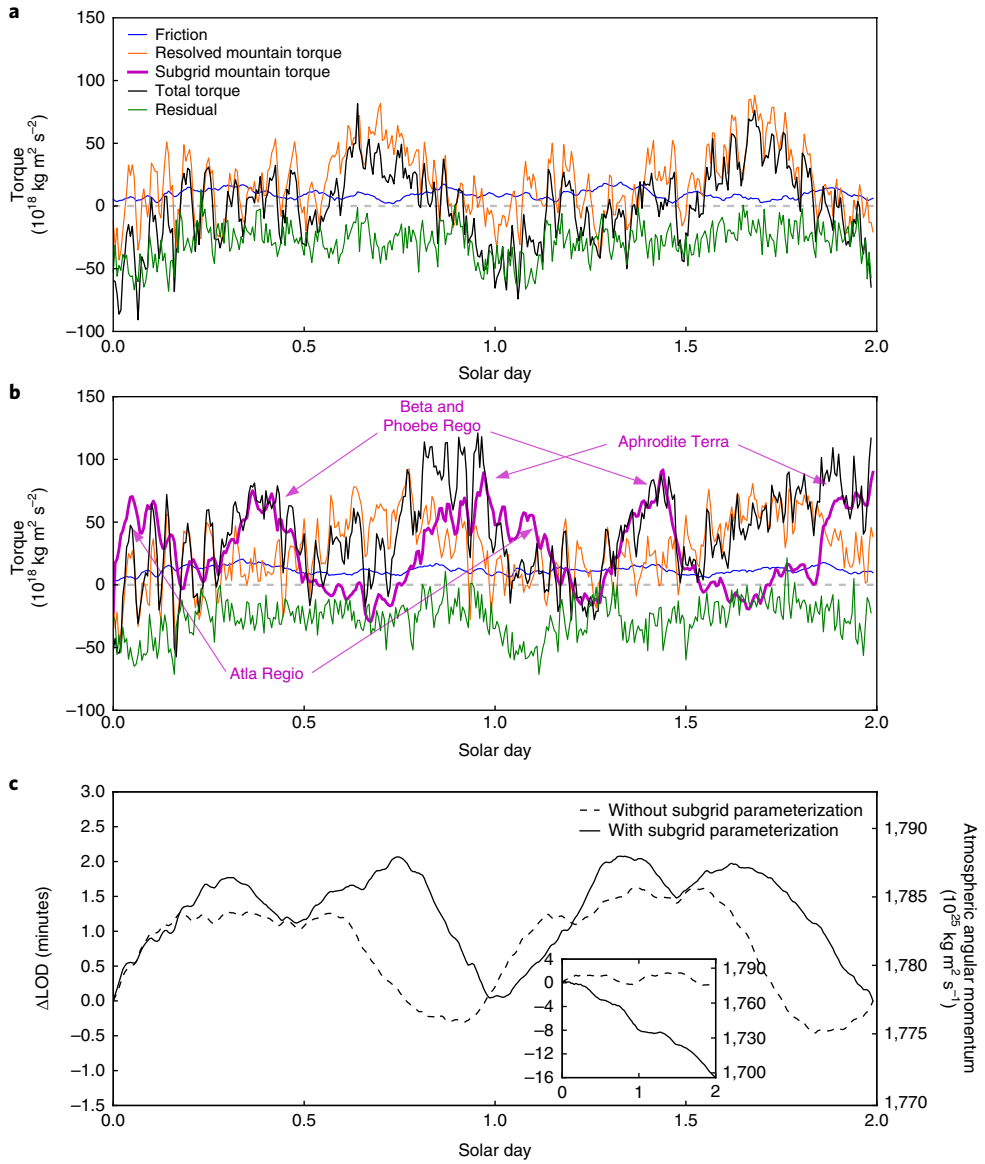

Fig. 3 | Atmospheric torques on the surface and length of day. a,**b**, Budget of torques, without (**a**) and with (**b**) subgrid parameterization, exerted by the atmosphere on the solid surface, and the resulting change in atmospheric angular momentum and length of day. The horizontal dashed line is the zero torque value. **c**, Intradiurnal fluctuations of length of sidereal day shown with their long-term trend removed. Inset: the total change of length of day shows the sustained loss of atmospheric momentum induced by mountain waves, leading to an unrealistic vertical profile of zonal wind (Supplementary Figs. 4 and 5).

Table 1 | Atmospheric torque budget

	$\overline{dM/dt}$	$\overline{GW}$	$\overline{T}$	$\overline{F}$	$\overline{\epsilon}$
Without parameterization	0.2 (90.5)	0 (0)	19.2 (131.1)	9.3	−28.8
With parameterization	−40.5 (97.8)	27.2 (120.9)	28.4 (146.1)	11.5	−26.6

Average of terms of the total angular momentum budget (units are 10^{18} kg m^2 s^{-2}; peak-to-peak amplitude is given in parenthesis). M is the total atmospheric angular momentum; hence dM/dt is the total atmospheric torque. The torques exerted by the atmosphere on the surface are the subgrid mountain torque (GW), the resolved mountain torque (T) and the friction torque (F). ϵ is the residual rate of angular momentum due to conservation errors in the dynamical core[13].

effects: a diurnal tide fixed with local time, and weaker baroclinic waves with a roughly five Earth days period carried by the atmospheric superrotation (Supplementary Fig. 7). These two effects are clearly apparent in the resolved mountain torque in Fig. 3 and Supplementary Fig. 7.

With the subgrid parameterization, a substantial contribution to the total atmospheric torque on the surface is the subgrid mountain torque. The subgrid mountain torque brings an additional positive contribution to the torques exerted on the surface. This torque would result in a change of LOD about 15 minutes if the torque exerted by the gravity wave were sustainable over a full solar day. The non-zero value of $\overline{dM/dt}$ shows that the simulation with the subgrid parameterization is not sustainable, and the atmosphere transfers most of its angular momentum to the solid body in a few

tens of days (Fig. 3 and Supplementary Fig. 4). The loss of angular momentum by planetary-scale gravity waves will eventually create a feedback on the near-surface winds, and reduce the subgrid mountain torque (Supplementary Fig. 5).

Although we are faced with a purely model-dependent issue of unrealistic angular momentum loss to conclude anything about the long-term budget of atmospheric angular momentum, some aspects of the different components of the mountain torque can be of interest to investigate the characteristics of the exchanges of angular momentum between the surface of Venus and its atmosphere. The subgrid mountain torque reflects physical processes on a kilometre length scale, while the resolved mountain torque happens at a 100 km to planetary length scale. To sum up, the intradiurnal change of the LOD due to the atmosphere is a combination of mainly three effects: the subgrid mountain torque generating planetary-scale stationary gravity waves induced by the diurnal cycle of near-surface stability; the eastward-propagating diurnal tide of surface pressure induced by the Sun; westward-propagating baroclinic waves with a period of five Earth days induced by the atmospheric superrotation at upper altitudes.

In a more complete model, the balance between the torques exerted by the Sun on the solid-body tide and on the atmospheric thermal tides would also need to be taken into account[16–19].

Due to the modelling limitations of atmospheric angular momentum conservation, it is not clear whether and how an interdiurnal fluctuation may exist. This calls for more observations of the planetary-scale stationary waves to spot any interdiurnal changes. Eventually, an accurate measurement of the LOD could detect the various impacts of the atmospheric flow against mountains. A good understanding of these underlying mechanisms could open the possibility of estimating the moment of inertia of Venus (for which no certain value exists so far), probing its interior, discovering the nature of its core, assessing the mechanisms involved in creating and maintaining the atmospheric superrotation, and exploring the evolution of the spin–orbit of Venus[20].

Methods

Methods, including statements of data availability and any associated accession codes and references, are available at https://doi.org/10.1038/s41561-018-0157-x.

Received: 17 October 2017; Accepted: 15 May 2018;
Published online: 18 June 2018

References

1. Fukuhara, T. et al. Large stationary gravity wave in the atmosphere of Venus. *Nat. Geosci.* **10**, 85–88 (2017).
2. Schubert G. in *Venus* (eds Hunten, D. M. et al.) 681–765 (Univ. Arizona Press, Tuscon, 1983).
3. Kouyama, T. et al. Topographical and local time dependence of large stationary gravity waves observed at the cloud top of Venus. *Geophys. Res. Lett.* **44**, 12098–12105 (2017).
4. Lebonnois, S. et al. Superrotation of Venus' atmosphere analyzed with a full general circulation model. *J. Geophys. R.* **115**, E06006 (2010).
5. Lebonnois, S., Sugimoto, N. & Gilli, G. Wave analysis in the atmosphere of Venus below 100-km altitude, simulated by the LMD Venus GCM. *Icarus* **278**, 38–51 (2016).
6. McFarlane, N. A. The effect of orographically excited gravity wave drag on the general circulation of the lower stratosphere and troposphere. *J. Atmos. Sci.* **44**, 1775–1800 (1987).
7. Lott, F. & Miller, M. J. A new subgrid-scale orographic drag parametrization: its formulation and testing. *Q. J. R. Meteorol. Soc.* **123**, 101–127 (1997).
8. Scinocca, J. F. & McFarlane, N. A. The parametrization of drag induced by stratified flow over anisotropic orography. *Q. J. R. Meteorol. Soc.* **126**, 2353–2393 (2000).
9. Collins, M., Lewis, S. R. & Read, P. L. Gravity wave drag in a global circulation model of the martian atmosphere: Parameterisation and validation. *Adv. Space Res.* **19**, 1245–1254 (1997).
10. Forget, F. et al. Improved general circulation models of the Martian atmosphere from the surface to above 80 km. *J. Geophys. Res.* **104**, 24155–24175 (1999).
11. Haus, R., Kappel, D. & Arnold, G. Atmospheric thermal structure and cloud features in the southern hemisphere of Venus as retrieved from VIRTIS/VEX radiation measurements. *Icarus* **232**, 232–248 (2014).
12. Miranda, P. M. A. & James, I. N. Non-linear three-dimensional effects on gravity-wave drag: splitting flow and breaking waves. *Q. J. R. Meteorol. Soc.* **118**, 1057–1081 (1992).
13. Lebonnois, S. et al. Angular momentum budget in General Circulation Models of superrotating atmospheres: a critical diagnostic. *J. Geophys. Res.* **117**, 12004 (2012).
14. Mueller, N. T., Helbert, J., Erard, S., Piccioni, G. & Drossart, P. Rotation period of Venus estimated from Venus Express VIRTIS images and Magellan altimetry. *Icarus* **217**, 474–483 (2012).
15. Cottereau, L., Rambaux, N., Lebonnois, S. & Souchay, J. The various contributions in Venus rotation rate and LOD. *Astron. Astrophys.* **531**, A45 (2011).
16. Gold, T. & Soter, S. Atmospheric tides and the resonant rotation of Venus. *Icarus* **11**, 356–366 (1969).
17. Takagi, M. & Matsuda, Y. Effects of thermal tides on the Venus atmospheric superrotation. *J. Geophys. Res.* **112**, D09112 (2007).
18. Leconte, J., Wu, H., Menou, K. & Murray, N. Asynchronous rotation of Earth-mass planets in the habitable zone of lower-mass stars. *Science* **347**, 632–635 (2015).
19. Auclair-Desrotour, P., Laskar, J., Mathis, S. & Correia, A. C. M. The rotation of planets hosting atmospheric tides: from Venus to habitable super-Earths. *Astron. Astrophys.* **603**, A108 (2017).
20. Correia, A. C. M. & Laskar, J. The four final rotation states of Venus. *Nature* **411**, 767 (2001).

Acknowledgements

We thank NASA for its financial support (grant NNX16AC84G) and the Akatsuki team for its discussions.

Author contributions

T.N. performed the simulations, model development and scientific interpretation; G.S. contributed to the scientific interpretation, and S.L. to the model development and simulations.

Competing interests

The authors declare no competing interests.

Additional information

Supplementary information is available for this paper at https://doi.org/10.1038/s41561-018-0157-x.

Reprints and permissions information is available at www.nature.com/reprints.

Correspondence and requests for materials should be addressed to T.N.

Publisher's note: Springer Nature remains neutral with regard to jurisdictional claims in published maps and institutional affiliations.

Methods

GCM. The IPSL Venus GCM is a full-physics GCM[4]. Its dynamical core is a finite-difference scheme on a latitude–longitude grid with a resolution of 96 by 96 points for this study. The vertical coordinates are sigma hybrid coordinates, with 50 levels extending from the surface to 5 Pa (100 km). At the poles, a classical Fourier filter is applied longitudinally poleward of 60° to limit the numerical instabilities of the coarse resolution in longitude. Horizontal dissipation is done with an iterated Laplacian, and a sponge layer absorbs reflection on the top of the model in the four uppermost layers. In the dynamical core and the physical parameterizations, the specific heat varies with temperature. The physics include a realistic topography, with data from Magellan at the model resolution. A Mellor and Yamada scheme is used for the boundary layer, improving the agreement with observations of temperature and winds from the surface to the bottom of the cloud deck[5]. The dry convection is parameterized, with the mixing of potential enthalpy. The radiative transfer is performed with look-up tables for solar radiation, and net exchange rate matrices for thermal radiation. The cloud structure is imposed between 47 km and its top, whose altitude is varying from the equator to the poles between 60 km and 70 km (ref. [21]). The thermal conduction in the soil is simulated with 11 underground layers with a constant thermal inertia (2,000 SI).

Subgrid-scale orographic parameterization. We implemented the effect of the subgrid-scale orography in the Venus GCM. We adapted an existing scheme[7] with the topography at a 4 km horizontal resolution from the Magellan radar mission[22]. At each model grid point, this scheme computes four parameters from the high-resolution topography found inside the boundaries of a model grid point: its standard deviation, anisotropy, slope and orientation (see Supplementary Fig. 9). For each grid point, near-surface quantities are defined as the average between the surface and half the standard deviation of the subgrid topography. From these four parameters, an ensemble of identical, idealized, elliptical mountains[23] is derived. The mountain stress is computed for this ensemble of mountains. Unlike other subgrid-scale schemes developed for Earth GCMs[6–8], the rationale for Venus is also to resolve at the GCM resolution large gravity waves induced by topographic obstacles not resolved by the GCM.

For that purpose, we modified this existing scheme[7], by considering that a gravity wave can be eventually resolved by the GCM. The value of the mountain stress is used as the criterion to determine whether a wave is resolved at the GCM resolution. Above a certain threshold, the wave can be resolved to the GCM dynamics by deposition of momentum at a fixed altitude. Below the threshold, complex and various processes can occur, with dispersion and superposition of subgrid waves that might eventually break. Assessing wave breaking is especially challenging for Venus, as the background flow generally increases with altitude. Incidentally, our initial tests of the implementation of this parameterization showed that the criterion for wave breaking used in an Earth GCM (when the Richardson number is smaller than 0.25) was often not satisfied on the whole atmospheric column.

Thus, two values need to be to chosen for this modified parameterization.

The first value is the threshold on the surface mountain stress to separate waves that are resolved by the GCM and waves that are not. From visual inspection of the mountain stress obtained from simulations, we chose this threshold to be 2 Pa, although dedicated theoretical studies could be done to fix this value. A value of 2 Pa distinguishes well the stress of high elevated terrains from the one of the plains (see Fig. 2 and Supplementary Fig. 2), and eventually make a good match with the time and location of the observed large-scale gravity waves.

The second value is the altitude at which a mountain wave is resolved by the GCM. This altitude is at the 19th layer of the model (that is, approximately 35 km). This particular altitude can be understood by a simple rule of thumb. The energy of the wave is concentrated along a parabola[23]:

$$y^2 = \frac{Nzax}{U}$$

This gives the-three dimensional shape of the mountain wave, where N is the Brunt–Väisälä frequency, U is the horizontal wind in the x-coordinates direction, and a is the size of the subgrid mountain. In this parameterization, a is given by the subgrid slope divided by the standard deviation. If x and y are taken as the horizontal resolution (that is, ~400 km), N and U as the averaged value in the deep atmosphere[2] (respectively $3.10^{-3}\,s^{-1}$ and $10\,m\,s^{-1}$), and with a having a typical size of 40 km, one finds an altitude $z = 33$ km. This altitude depends on the horizontal resolution of the model. At this altitude and above, the perturbation caused by the gravity wave mountain stress is wide enough to be resolved at the model resolution. As a result of the fact that the horizontal dimension of mountain wave perturbation grows with altitude, an increased (decreased) horizontal resolution would require a lower (higher) altitude.

However, U and N vary with height, and the wave actually extends outside the region of the parabola, although most of its energy is confined to it. Therefore, this rule of thumb only simply and crudely justifies the retained altitude of 35 km. Other values for this altitude are investigated (see Supplementary Information), and a lower altitude does not create a planetary-scale wave observed at the cloud top.

In the end, the gravity wave mountain stress of the parameterization is released at 35 km for values greater than 2 Pa, as follows:

$$\frac{du}{dt} = -g\cos(\alpha)\frac{\tau}{\Delta p} \quad (1)$$

$$\frac{dv}{dt} = -g\sin(\alpha)\frac{\tau}{\Delta p} \quad (2)$$

where τ is the stress, Δp is the pressure difference between the mid-layers above and below the altitude of stress release, g is the gravitational acceleration and α is the angle between the near-surface wind and the direction of the stress. The tunable parameters of this parameterization are the gravity wave drag coefficient G (ref. [24]), the inverse critical Froude number H_{nc}, and the drag coefficient C_d. G is a scalar defined for an elliptically shaped mountain and depends solely on the mountain sharpness. H_{nc} defines the maximal altitude z_b at which the blocked-flow stress is applied, via $z_b = H - UN^{-1}H_{nc}$. C_d is the classical drag coefficient, and the blocked flow stress is proportional to it. The retained values are the same as for Earth[7], with H_{nc}, $C_d = 1$, and Mars[9], with $G = 1$. A fourth parameter, the critical Richardson number, is not present for this adaptation to Venus, since the effect of the breaking is instead simulated more crudely by stress released at the lowest grid point.

Code availability. All model versions are available upon request by contacting the corresponding author.

Data availability. All simulations results are available upon request by contacting the corresponding author.

References

21. Garate-Lopez, I. & Lebonnois, S. Impacts of the cloud structure's latitudinal variation on the general circulation of the Venus atmosphere as modeled by the LMD-GCM. EGU Geophys. *Res. Abstracts* **19**, 12972 (2017).
22. Ford, P. G. & Pettengill, G. H. Venus topography and kilometer-scale slopes. *J. Geophys. Res.* **97**, 13103–13114 (1992).
23. Smith, R. B. Linear theory of stratified hydrostatic flow past an isolated mountain. *Tellus* **32**, 348–364 (1980).
24. Phillips, D. S. Analytical surface pressure and drag for linear hydrostatic flow over three-dimensional elliptical mountains. *J. Atmos. Sci.* **41**, 1073–1084 (1984).